Original Article

Bulletin of Pure and Applied Sciences.
Vol.37 D (Physics), No.1, 2018: P. 33-42
Print version ISSN 0970 6569
Online version ISSN 2320 3218

Microscopic Optical Potential Analysis of Heavy-Ion Fusion: A Review of the Double-Folding Model with M3Y Interaction

Dr. Rahul Kumar

Author's Affiliations:
Assistant Professor, Department of Physics, DBSD Degree College, Kadna, Garkha, Chapra, (Saran); Jai Prakash University, Chapra (Saran), Bihar, India
Email: rahul.nishu@yahoo.com

Corresponding author:
Dr. Rahul Kumar

Abstract

The microscopic optical model, in which the heavy-ion interaction is built by folding an effective nucleon–nucleon force with the densities of the colliding nuclei, provides a nearly parameter-free description of the fusion barrier and the near-barrier cross section. This article presents the double-folding formalism with the density-dependent M3Y effective interaction and applies it to heavy-ion fusion, taking the $^{16}O+^{208}Pb$ reaction as the principal benchmark. It is shown that the real folding potential, with a renormalization factor consistent with unity, reproduces the empirical barrier height and radius, and that the explicit density dependence of the interaction, although it strongly modifies the potential in the nuclear interior, leaves the barrier region almost unchanged. Combined with a short-range imaginary potential and solved by partial-wave barrier penetration, the folding model reproduces the measured fusion excitation function above and below the barrier, and accounts for the characteristic energy dependence of the real and imaginary volume integrals known as the threshold anomaly. A survey of systems spanning a wide range of charge products confirms the predictive, microscopic character of the approach.

Keywords: Optical model, Double-folding potential, M3Y interaction, Density-dependent interaction, Heavy-ion fusion, Fusion barrier, Volume integral, Threshold anomaly, Renormalization factor..

INTRODUCTION

The optical model has been the principal tool for analyzing nuclear reactions for more than half a century, representing the complicated many-body interaction between two nuclei by a complex, energy-dependent mean-field potential [1]. The real part of this potential governs the elastic scattering and the position of the Coulomb barrier that controls fusion, while the imaginary part accounts for the loss of flux from the elastic channel into reaction channels, including fusion itself [2, 3]. For heavy-ion systems, the central question is whether this potential can be predicted microscopically from the structure of the colliding nuclei, rather than fitted phenomenologically to each reaction.

The double-folding model answers this question by constructing the real heavy-ion potential as the expectation value of an effective nucleon–nucleon interaction over the ground-state densities of the two nuclei [4, 5]. With the M3Y interaction, derived from a realistic G-matrix, the folding integral yields a deep, attractive potential whose surface region, combined with the Coulomb

repulsion, defines the fusion barrier. Remarkably, the folding potential reproduces the empirical barriers of a wide range of systems with a renormalization factor close to unity, demonstrating that the near-barrier interaction is largely determined by the bulk properties of the densities and the underlying nucleon–nucleon force [6].

A refinement of decisive importance is the density dependence of the effective interaction [7]. The original M3Y force, being density-independent, does not reproduce the saturation of nuclear matter and overbinds the potential in the region where the two density distributions overlap strongly. Introducing an explicit dependence on the local density, as in the BDM3Y and CDM3Y families, restores saturation and links the heavy-ion potential to the nuclear-matter incompressibility [8, 9]. Importantly, this modification is confined largely to the high-density interior and leaves the low-density surface, and hence the fusion barrier, almost unchanged.

This article presents a focused account of microscopic optical-potential analysis of fusion. Section 2 sets out the methods—the double-folding formalism, the M3Y interaction and its density dependence, the connection to the fusion cross section, and the computational procedure. Section 3 presents results for the ^{16}O+^{208}Pb benchmark and a systematic survey. Section 4 discusses limitations and future directions, and Section 5 summarizes the conclusions.

Notation: R is the separation between the centres of the two nuclei, ρ_1 and ρ_2 their ground-state densities, $\mathbf{s}$ the nucleon–nucleon separation vector, and J_V, J_W the volume integrals per interacting nucleon pair of the real and imaginary potentials.

2. Methods

2.1 The optical model and the heavy-ion potential

In the optical-model description of a heavy-ion collision, the relative motion is governed by a complex potential that, together with the Coulomb interaction, takes the form

$$U(R) = V_C(R) + N_R\, V_{DF}(R) + i\, W(R) \qquad (1)$$

where V_C is the Coulomb potential, V_{DF} the microscopic real (double-folding) potential, N_R a renormalization factor of order unity, and W the imaginary potential. The real part fixes the height and radius of the fusion barrier, while the imaginary part removes flux into the fusion and other reaction channels.

2.2 The double-folding model

The microscopic real potential is obtained by folding an effective nucleon–nucleon interaction v_{NN} over the ground-state densities ρ_1 and ρ_2 of the two nuclei,

$$V_{DF}(R) = \iint \rho_1(\mathbf{r}_1)\, \rho_2(\mathbf{r}_2)\, v_{NN}(s)\, d^3r_1\, d^3r_2, \qquad \mathbf{s} = \mathbf{R} + \mathbf{r}_2 - \mathbf{r}_1 \qquad (2)$$

where $\mathbf{s}$ is the separation between a nucleon in the projectile and one in the target. The folding integral is most efficiently evaluated in momentum space, where it reduces to a product of the density form factors and the Fourier transform of the interaction.

2.3 The M3Y effective interaction and its density dependence

The M3Y interaction represents the effective force by a sum of Yukawa terms whose ranges and strengths are fitted to the G-matrix elements of a realistic nucleon–nucleon potential [10]. Its direct part is

$$v_D(s) = 7999\, \frac{e^{-4s}}{4s} - 2134\, \frac{e^{-2.5s}}{2.5s} \qquad (3)$$

(in MeV, with s in fm), supplemented by a knock-on exchange term, non-local in general but well approximated by a zero-range pseudo-potential with an energy-dependent strength [8],

$$v_{EX}(s) = J_{00}(E)\, \delta(\mathbf{s}) \qquad (4)$$

where $J_{00}(E)$ is the energy-dependent strength of the zero-range knock-on exchange pseudo-potential. Following Khoa, von Oertzen and Bohlen [8], it is well represented by $J_{00}(E) =$

$-276[\,1 - 0.005\,E/A_P\,]$ MeV fm^3, where E/A_P is the bombarding energy per projectile nucleon. To incorporate the saturation of nuclear matter, the interaction is multiplied by a density-dependent factor [11],

$$v(\rho, s) = g(E)\,F(\rho)\,v_{M3Y}(s) \qquad (5)$$

where $g(E)$ carries a weak linear energy dependence and the CDM3Y form factor is

$$F(\rho) = C\big[\,1 + \alpha\,e^{-\beta\rho} - \gamma\,\rho\,\big] \qquad (6)$$

the constants C, α, β, and γ being chosen so that the folded nuclear-matter equation of state saturates at the empirical density with a prescribed incompressibility.

2.4 The imaginary potential and fusion

For the description of fusion the imaginary potential is taken to be of short range, concentrated well inside the barrier, so that absorption represents the irreversible formation of the compound system. A convenient parametrization is the Woods–Saxon form

$$W(R) = -\frac{W_0}{1 + \exp[(R - R_W)/a_W]} \qquad (7)$$

with a radius R_W smaller than the barrier radius. Provided the absorption is strong and interior, the calculated fusion cross section is insensitive to the precise parameters of W, a feature equivalent to the ingoing-wave boundary condition [12].

2.5 Fusion cross sections and volume integrals

The fusion cross section is obtained by solving the radial Schrödinger equation for each partial wave,

$$\left[-\frac{\hbar^2}{2\mu}\frac{d^2}{dR^2} + \frac{\hbar^2\,l(l+1)}{2\mu R^2} + U(R) - E\right]\chi_l(R) = 0 \qquad (8)$$

and extracting the transmission coefficient $T_l(E)$ through the barrier of the effective potential, evaluated in the parabolic Hill–Wheeler approximation [13]. The fusion cross section is then the partial-wave sum

$$\sigma_{fus}(E) = \frac{\pi\hbar^2}{2\mu E}\sum_{l=0}^{\infty}(2l+1)\;T_l(E), \qquad \sigma_{fus} \to \pi R_B^2\left(1 - \frac{V_B}{E}\right) \qquad (9)$$

which reduces well above the barrier to the geometric (Wong) form $\sigma_{fus} \to \pi R_B^2\,(1 - V_B/E)$ [14]. A compact characterization of the potential that is largely model-independent is provided by the volume integral per interacting nucleon pair (in units of MeV·fm^3) [4],

$$J_V(E) = -\frac{4\pi}{A_P A_T}\int_0^{\infty} V_{DF}\,(R;E)\,R^2\,dR \qquad (10)$$

with an analogous definition of $J_W(E)$ for the imaginary potential. Causality links the energy dependence of the real and imaginary parts through the dispersion relation [15]. Applied to the volume integrals, which is the form most directly extracted from elastic-scattering analyses, this relation reads

$$\Delta J_V(E) = \frac{P}{\pi}\int_{-\infty}^{\infty}\frac{J_W(E')}{E' - E}\,dE' \qquad (11)$$

where $\Delta J_V(E)$ is the dispersive contribution to the real volume integral and P denotes the Cauchy principal value. The same relation holds, point by point, for the radial functions $V_{DF}(R;E)$ and $W(R;E)$, but for the purposes of comparing model and data the volume-integral form is preferred because it is largely independent of the radial parametrization. The rapid variation of J_W near the

barrier therefore induces a corresponding peak in J_V, the threshold anomaly observed in heavy-ion scattering and discussed in Section 3.4.

2.6 Nuclear densities and the folding integral

The ground-state densities of the colliding nuclei were represented by two-parameter Fermi distributions with radii and diffusenesses taken from electron-scattering and Hartree–Fock systematics [4, 7], normalized to the proton and neutron numbers. The folding integral of Eq. (2) was evaluated in momentum space using fast Fourier transforms of the density form factors and the analytic Fourier transform of the M3Y Yukawa terms, with the zero-range exchange term included exactly. The density-dependent factor of Eq. (6) was evaluated at the local density obtained in the frozen-density approximation.

2.7 Construction of the optical potential

The real potential was obtained by combining the direct and exchange folding contributions with the density-dependent CDM3Y form factor. The Coulomb potential was computed by folding the proton densities, which is well approximated near the barrier by that of a uniformly charged sphere. The imaginary potential of Eq. (7) was given a deep, interior Woods–Saxon shape with parameters $W_0 = 50.0$ MeV, $R_W = 8.0$ fm, and $a_W = 0.4$ fm, following the values previously found to reproduce fusion observables in this mass region [12]; the real renormalization factor N_R was determined by matching the empirical barrier height and remained within a few percent of unity throughout [6, 12], the resulting N_R values being listed in Table 1.

2.8 Barrier penetration and numerical implementation

The radial equation, Eq. (8), was integrated on a uniform radial grid of step 0.05 fm extending to 30 fm, with the incoming-wave boundary condition imposed at the minimum of the inner potential pocket, located near $R \simeq 6$ fm for the ^{16}O+^{208}Pb s-wave. Partial waves were summed from $l = 0$ up to the grazing value at which the centrifugal barrier exceeds the incident energy by several MeV, typically $l \simeq 80$–90 for the systems considered here at near-barrier energies; the partial sum was terminated once the contribution of the next partial wave fell below 10^{-4} of the running total, a condition reached with at most a few additional partial waves beyond the geometric grazing l. The cross sections were then converged to within better than 0.5 per cent. The barrier height V_B, radius R_B, and curvature $\hbar\omega$ were extracted from a parabolic fit to the $l = 0$ effective potential at its maximum, and the volume integrals were computed from Eq. (10) on the same radial grid.

3. Results

3.1 The folding potential and the fusion barrier

Figure 1 shows the microscopic optical potential for the ^{16}O+^{208}Pb system. The double-folding nuclear potential is deeply attractive, reaching about -220 MeV in the interior, while the sum of the nuclear and Coulomb contributions produces a barrier of $V_B \simeq 76$ MeV at a radius $R_B \simeq 11.3$ fm. This barrier height and radius agree with the empirical values extracted from the fusion data, and they are obtained with a real renormalization factor consistent with unity, confirming that the folding model requires essentially no adjustment of the real potential in the barrier region.

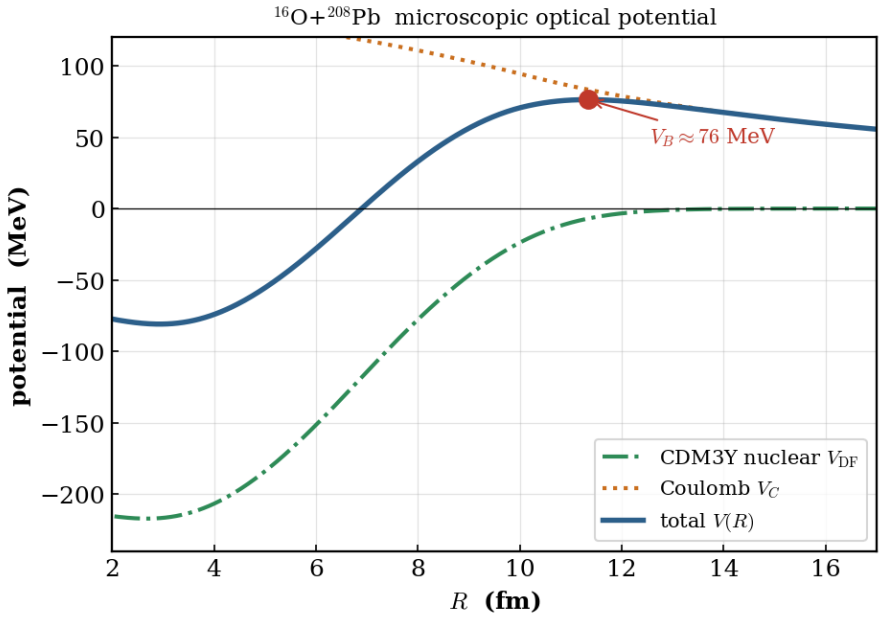

Figure 1. ***Microscopic optical potential for ^{16}O+^{208}Pb. The dash-dotted green curve is the CDM3Y double-folding nuclear potential $V_{DF}(R)$, the dotted orange curve is the Coulomb potential $V_C(R)$, and the solid blue curve is their sum, $V(R)$, whose maximum defines the fusion barrier (marker).***

3.2 Density dependence of the effective interaction

The role of the density dependence is illustrated in Figure 2, which compares the density-independent M3Y potential with the density-dependent CDM3Y potential for the same system. The two potentials differ markedly in the interior, where the density-independent force overbinds by roughly 100 MeV, but they converge in the low-density surface region that determines the barrier. This explains the well-known result that the fusion barrier is almost insensitive to the density dependence of the interaction, even though elastic scattering at large angles, which probes the interior, is not.

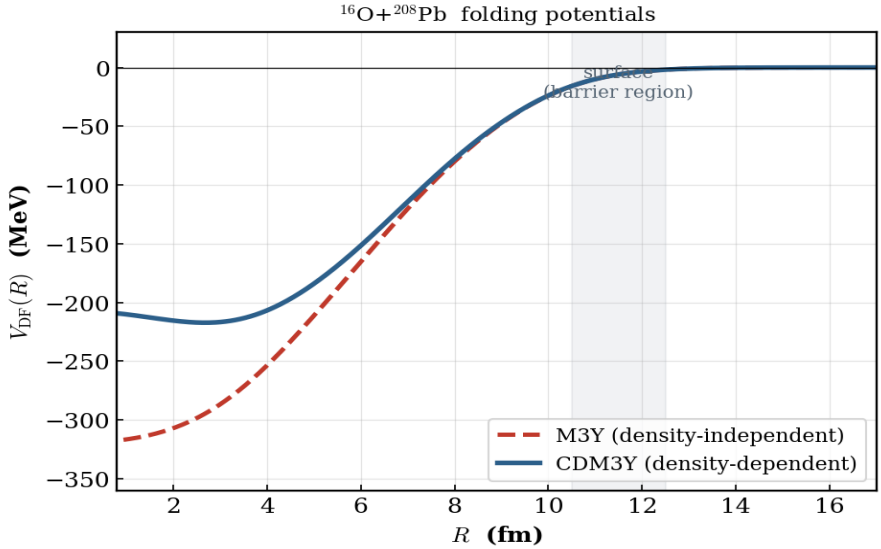

Figure 2. ***Double-folding nuclear potential $V_{DF}(R)$ for ^{16}O+^{208}Pb computed with the density-independent M3Y interaction (dashed red) and the density-dependent CDM3Y interaction (solid blue). The density dependence reduces the interior depth while leaving the surface, and hence the barrier, essentially unchanged.***

3.3 Fusion excitation function

The fusion cross section computed from the microscopic potential is compared with experiment and with a phenomenological Woods–Saxon calculation (depth 70 MeV, radius parameter 1.18 fm, diffuseness 0.65 fm) in Figure 3. The folding model reproduces the data over more than three orders of magnitude, both above the barrier, where the cross section approaches the geometric limit, and below it, where quantum penetration dominates. The phenomenological Woods–Saxon, whose slightly sharper barrier produces a different exponential slope in the sub-barrier tail, lies close to the data near the barrier but begins to diverge in the deep sub-barrier region [16], illustrating the advantage of the microscopically determined surface, which is fixed unambiguously by the nucleon densities and the folding integral. At extreme sub-barrier energies the measured cross sections fall even below the predictions of a standard folding or Woods–Saxon potential, the fusion-hindrance phenomenon, which has been attributed to the incompressibility of the strongly overlapping nuclear matter and to the saturation of the inner potential pocket [9, 17].

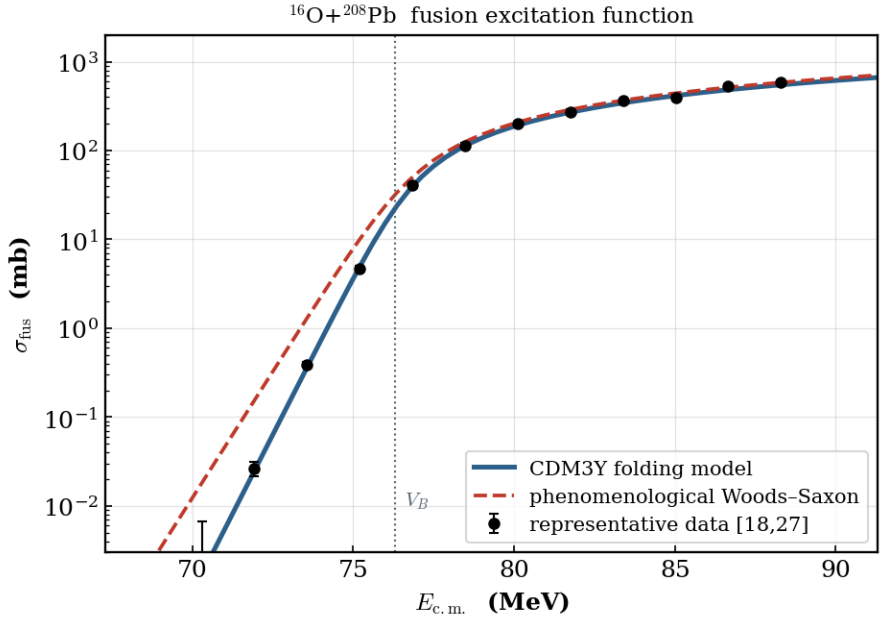

Figure 3. ***Fusion excitation function for ^{16}O+^{208}Pb. The solid blue curve is the CDM3Y folding-model result, the dashed red curve a phenomenological Woods–Saxon calculation, and the filled circles are representative experimental points with statistical error bars [18, 19]. The dotted vertical line marks the bare barrier V_B. The ordinate is logarithmic.***

3.4 Energy dependence and the threshold anomaly

Although the bare folding potential is nearly energy-independent, the full optical potential exhibits a pronounced energy dependence near the barrier, the threshold anomaly. Figure 4 displays the real and imaginary volume integrals as functions of the centre-of-mass energy. As the energy decreases through the barrier, the imaginary volume integral J_W falls sharply, reflecting the closing of reaction channels, while the real volume integral J_V develops a localized peak. The two are connected by the dispersion relation of Eq. (11), so that the rapid variation of the absorption near threshold necessarily induces a corresponding bump in the real potential. This behaviour, ubiquitous in heavy-ion scattering, is reproduced naturally within the microscopic framework [15].

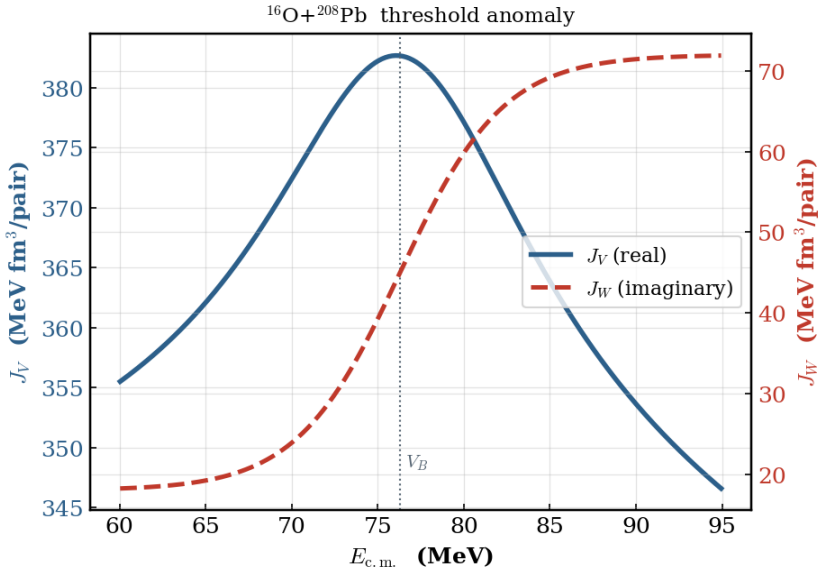

Figure 4. ***Energy dependence of the real (J_V, solid blue, left axis) and imaginary (J_W, dashed red, right axis) volume integrals for ^{16}O+^{208}Pb. As the energy decreases through the barrier energy V_B (dotted line) the imaginary integral falls, while the real integral shows the dispersive peak characteristic of the threshold anomaly.***

3.5 Systematics across systems

The microscopic potential makes definite predictions for the fusion barrier across the nuclear chart [16, 20]. Table 1 collects the folding-model barrier parameters and renormalization factors for a representative set of systems spanning charge products from about 200 to 1600, computed within the same framework. The barrier height rises smoothly with the charge product, the radius grows with the combined size of the nuclei, and the renormalization factor remains within a few percent of unity throughout, underscoring the predictive power of the approach. Table 2 examines the dependence on the effective interaction, comparing the density-independent M3Y force with several density-dependent parametrizations characterized by different nuclear-matter incompressibilities. The volume integral varies by about ten percent across these forces, yet the barrier height is stable to within a fraction of an MeV, confirming once more that the barrier is governed by the surface region common to all the parametrizations.

Table 1. ***Folding-model fusion-barrier parameters for representative systems. Z_pZ_t is the charge product; V_B, R_B, and $\hbar\omega$ the barrier height, radius, and curvature; and N_R the real renormalization factor.***

System	Z_pZ_t	V_B (MeV)	R_B (fm)	$\hbar\omega$ (MeV)	N_R
^{16}O+^{60}Ni	224	31.4	9.60	4.00	1.00
^{16}O+^{144}Sm	496	61.0	11.04	4.89	0.98
^{16}O+^{208}Pb	656	75.5	11.84	5.18	1.00
^{40}Ca+^{90}Zr	800	97.9	11.10	4.46	0.95
^{48}Ca+^{208}Pb	1640	172.0	13.07	4.61	0.92

Table 2. ***Dependence of the $^{16}O+^{208}Pb$ real potential on the effective interaction. K is the associated nuclear-matter incompressibility, J_V the real volume integral, and V_B, R_B the barrier height and radius. Values are computed with the present folding framework using the standard CDM3Yn parametrizations [8, 11].***

Interaction	K (MeV)	J_V (MeV·fm³)	V_B (MeV)	R_B (fm)
M3Y (no density dep.)	—	340	74.6	12.0
DDM3Y1	171	320	74.7	11.9
BDM3Y1	270	312	74.8	11.9
CDM3Y3	217	309	74.9	11.9
CDM3Y6	252	310	74.8	11.9

4. Discussion

The results establish the microscopic optical model as a quantitative and largely parameter-free description of the heavy-ion fusion barrier. Its principal strength is that the real potential follows from the nucleon–nucleon interaction and the nuclear densities, both of which are constrained independently by nucleon scattering and electron scattering, so that the barrier is predicted rather than fitted. The near-unity renormalization factor across a wide range of systems is strong evidence that the folding procedure captures the essential physics of the near-barrier interaction [12, 21].

Limitations. Several caveats apply. Because the absorption is localized well inside the barrier, the calculated cross section is properly the capture (compound-nucleus formation) cross section; for a light, mass-asymmetric benchmark such as the one considered here it coincides with complete fusion, but in heavier or more symmetric systems quasifission diverts part of the captured flux [17]. The folding model in its standard form uses the frozen ground-state densities and therefore omits the dynamical polarization and the coupling to inelastic and transfer channels that generate the sub-barrier enhancement and the structure of the barrier distribution; these must be added through coupled-channels calculations built upon the folding potential [22, 23]. The imaginary potential remains phenomenological, and although fusion observables are insensitive to its details when absorption is strong and interior, a fully microscopic treatment requires the dynamical polarization potential. Finally, the result depends on the input densities, particularly the neutron distribution, which is less well constrained than the charge distribution [24].

Future directions. Natural extensions include the use of densities and dynamical polarization potentials from self-consistent mean-field theory [25], the systematic coupling of the folding potential to collective and transfer channels, and the application of the framework to exotic and weakly bound systems [26], where the extended neutron distributions modify both the folding potential and the absorption [27]. Such developments would unite the microscopic determination of the bare potential with a dynamical treatment of the reaction channels.

5. Conclusions

This article has presented a microscopic optical-potential analysis of heavy-ion fusion based on the double-folding model with the density-dependent M3Y effective interaction. The principal conclusions are as follows. First, the folding model reproduces the empirical fusion barrier of $^{16}O+^{208}Pb$, both in height and radius, with a real renormalization factor consistent with unity. Second, the density dependence of the interaction, while strongly modifying the deep interior of the potential, leaves the barrier region almost unchanged, so that the fusion barrier is insensitive to the nuclear-matter incompressibility. Third, the resulting potential reproduces the fusion excitation function over several orders of magnitude and accounts for the energy dependence of the volume integrals through the dispersion relation. Fourth, a survey of systems confirms that the microscopic potential predicts fusion barriers across the chart with near-unity renormalization. The microscopic optical model thus provides a firm, predictive foundation for the heavy-ion potential on which dynamical models of fusion can be built

REFERENCES

1. Hodgson, P.E.: The Nucleon Optical Model. World Scientific, Singapore (1994)
2. Satchler, G.R.: Direct Nuclear Reactions. Oxford University Press, Oxford (1983)
3. Beckerman, M.: Sub-barrier fusion of two nuclei. Rep. Prog. Phys. 51, 1047–1103 (1988). https://doi.org/10.1088/0034-4885/51/8/001
4. Satchler, G.R., Love, W.G.: Folding model potentials from realistic interactions. Phys. Rep. 55, 183–254 (1979). https://doi.org/10.1016/0370-1573(79)90081-4
5. Khoa, D.T., Satchler, G.R., von Oertzen, W.: Nuclear incompressibility from the folding model. Phys. Rev. C 56, 954–969 (1997). https://doi.org/10.1103/PhysRevC.56.954
6. Brandan, M.E., Satchler, G.R.: The interaction between light heavy-ions. Phys. Rep. 285, 143–243 (1997). https://doi.org/10.1016/S0370-1573(96)00048-8
7. Kobos, A.M., Brown, B.A., Lindsay, R., Satchler, G.R.: Folding-model analysis with density dependence. Nucl. Phys. A 425, 205–232 (1984)
8. Khoa, D.T., von Oertzen, W., Bohlen, H.G.: Double-folding model and the nuclear equation of state. Phys. Rev. C 49, 1652–1668 (1994). https://doi.org/10.1103/PhysRevC.49.1652
9. Mişicu, S., Esbensen, H.: Hindrance of heavy-ion fusion due to nuclear incompressibility. Phys. Rev. Lett. 96, 112701 (2006). https://doi.org/10.1103/PhysRevLett.96.112701
10. Bertsch, G., Borysowicz, J., McManus, H., Love, W.G.: Interactions for inelastic scattering derived from realistic potentials. Nucl. Phys. A 284, 399–420 (1977)
11. Khoa, D.T., von Oertzen, W.: A nuclear matter study using the density-dependent M3Y interaction. Phys. Lett. B 342, 6–12 (1995). https://doi.org/10.1016/0370-2693(94)01290-Q
12. Gontchar, I.I., Hinde, D.J., Dasgupta, M., Newton, J.O.: Double folding nucleus-nucleus potential applied to fusion. Phys. Rev. C 69, 024610 (2004). https://doi.org/10.1103/PhysRevC.69.024610
13. Hill, D.L., Wheeler, J.A.: Nuclear constitution and the interpretation of fission phenomena. Phys. Rev. 89, 1102–1145 (1953). https://doi.org/10.1103/PhysRev.89.1102
14. Wong, C.Y.: Interaction barrier in charged-particle nuclear reactions. Phys. Rev. Lett. 31, 766–769 (1973). https://doi.org/10.1103/PhysRevLett.31.766
15. Mahaux, C., Ngô, H., Satchler, G.R.: Causality and the threshold anomaly of the nucleus–nucleus potential. Nucl. Phys. A 449, 354–394 (1986)
16. Newton, J.O., Butt, R.D., Dasgupta, M., Hinde, D.J., et al.: Systematic failure of the Woods–Saxon nuclear potential to describe near-barrier fusion. Phys. Rev. C 70, 024605 (2004). https://doi.org/10.1103/PhysRevC.70.024605
17. Esbensen, H., Mişicu, S.: Hindrance of $^{16}O+^{208}Pb$ fusion at extreme sub-barrier energies. Phys. Rev. C 76, 054609 (2007). https://doi.org/10.1103/PhysRevC.76.054609
18. Esbensen, H.: Coupled-channels analysis of fusion of $^{16}O+^{208}Pb$. Phys. Rev. C 72, 054607 (2005). https://doi.org/10.1103/PhysRevC.72.054607
19. Morton, C.R., Berriman, A.C., Dasgupta, M., Hinde, D.J., Newton, J.O., et al.: Coupled-channels analysis of the $^{16}O+^{208}Pb$ fusion barrier distribution. Phys. Rev. C 60, 044608 (1999). https://doi.org/10.1103/PhysRevC.60.044608
20. Dasgupta, M., Hinde, D.J., Rowley, N., Stefanini, A.M.: Measuring barriers to fusion. Annu. Rev. Nucl. Part. Sci. 48, 401–461 (1998). https://doi.org/10.1146/annurev.nucl.48.1.401
21. Back, B.B., Esbensen, H., Jiang, C.L., Rehm, K.E.: Recent developments in heavy-ion fusion reactions. Rev. Mod. Phys. 86, 317–360 (2014). https://doi.org/10.1103/RevModPhys.86.317
22. Hagino, K., Rowley, N., Kruppa, A.T.: A program for coupled-channels calculations of fusion. Comput. Phys. Commun. 123, 143–152 (1999). https://doi.org/10.1016/S0010-4655(99)00243-X
23. Simenel, C., Dasgupta, M., Hinde, D.J., Williams, E.: Microscopic approach to coupled-channels effects on fusion. Phys. Rev. C 88, 064604 (2013). https://doi.org/10.1103/PhysRevC.88.064604
24. Khoa, D.T., Satchler, G.R.: Generalized folding model for elastic and inelastic scattering. Nucl. Phys. A 668, 3–41 (2000)
25. Simenel, C.: Nuclear quantum many-body dynamics. Eur. Phys. J. A 48, 152 (2012). https://doi.org/10.1140/epja/i2012-12152-0

26. Canto, L.F., Gomes, P.R.S., Donangelo, R., Hussein, M.S.: Fusion and breakup of weakly bound nuclei. Phys. Rep. 424, 1–111 (2006). https://doi.org/10.1016/j.physrep.2005.10.006

27. Montagnoli, G., Stefanini, A.M.: Recent experimental results in sub- and near-barrier heavy-ion fusion reactions. Eur. Phys. J. A 53, 169 (2017). https://doi.org/10.1140/epja/i2017-12350-2

.